TECHNICAL NOTE

Experimental Evaluation of the In-Plane Stiffness of Timber Diaphragms

Anna Brignola,[a] Stefano Pampanin,[b] and Stefano Podestà[c]

The seismic response of unreinforced masonry (URM) buildings, in both their as-built or retrofitted configuration, is strongly dependent on the characteristics of wooden floors and, in particular, on their in-plane stiffness and on the quality of wall-to-floor connections. As part of the development of alternative performance-based retrofit strategies for URM buildings, experimental research has been carried out by the authors at the University of Canterbury, in order to distinguish the different elements contributing to the whole diaphragm's stiffness. The results have been compared to the ones predicted through the use of international guidelines in order to highlight shortcomings and qualities and to propose a simplified formulation for the evaluation of the stiffness properties. [DOI: 10.1193/1.4000088]

INTRODUCTION

Structures with flexible floor systems might behave differently during earthquakes than structures with rigid diaphragms. International guidelines on the seismic rehabilitation of buildings (ASCE/SEI 41-06 2007, NZSEE 2006, NTC 2008) and international literature (Tena-Colunga 1992, Tena-Colunga and Abrams 1996) underline the importance of correctly including the diaphragm flexibility and the wall-to-floor connections properties when modeling the response of unreinforced masonry (URM) buildings. Experimental (Paquette and Bruneau 2006) and numerical (Gattesco et al. 2007) research has been carried out, in order to better understand the real interaction between flexible floors and rigid walls.

It is particularly important to correctly evaluate the in-plane mechanical properties of timber diaphragms in both their as-built and retrofitted configurations. Some codes provide reference stiffness values for different types of timber floors, while others propose simplified analytical procedures to determine the in-plane stiffness, starting from the geometrical and mechanical characteristics of the floor. In no cases is the different behavior of the floor in the direction perpendicular to the joists well-specified. Few experimental results (Peralta et al. 2004, Piazza et al. 2008, Corradi et al. 2006) are available to support such empirical values or evaluation procedures, although different test setups have been adopted, with dissimilar boundary conditions, aspect ratios, types of floor and measured parameters. There is a clear need to homogenize the experimental results obtained during previous studies and the stiffness values evaluated by using different international codes through standard

[a] Dep. of Civil, Environmental and Architectural Engineering, University of Genoa, Italy
[b] Dep. of Civil and Natural Resources Engineering, University of Canterbury, Christchurch, New Zealand
[c] Dep. of Civil, Environmental and Architectural Engineering, University of Genoa, Italy

Earthquake Spectra, Volume 28, No. 4, pages 1–23, November 2012; © 2012, Earthquake Engineering Research Institute

reference values or simplified analytical procedures. This suggested the plan for an experimental program capable of distinguishing the stiffness contribution related to each different diaphragm's physical components (e.g., boards, panels, nails, screws).

As part of a joint project between the University of Canterbury and the University of Genoa on the development of alternative performance-based retrofit strategies for URM buildings (Brignola et al. 2009a, 2009b, 2010), a series of quasi-static cyclic tests on different diaphragm configurations have been carried out at the Structural Laboratory of the University of Canterbury. Attention during the definition of the experimental program was focused on the role of the wall-to-diaphragm connection (Brignola 2009). The comparison between experimental results and predictions allowed us to recognize shortcomings and qualities of current international code and guideline approaches, as well as to propose a simplified analytical approach for the evaluation of the in-plane stiffness properties of few types of timber diaphragms.

EVALUATION OF DIAPHRAGM STIFFNESS THROUGH THE USE OF INTERNATIONAL GUIDELINES

Different approaches are proposed by different international codes and guidelines on seismic rehabilitation of buildings with regard to the mathematical modeling methods to use in describing the diaphragms behavior during the seismic assessment of URM buildings. In this section, a comparison between the U.S., New Zealand, and Italian approaches is provided, in order to underline discrepancies and similarities arising from the different methodologies, while also highlighting the strengths and aspects that require further improvements.

THE ASCE APPROACH

The Structural Engineering Institute (SEI) of the American Society of Civil Engineers (ASCE) rearranged two Federal Emergency Management Agency (FEMA) documents, leading to the ASCE/SEI 31-03 (2003) and the ASCE/SEI 41-06 (2007) Standards on the Seismic Evaluation and the Rehabilitation of Existing Buildings, respectively. In ASCE/SEI 31-03, a definition of flexible and rigid diaphragms is suggested, related to the ratio between the maximum lateral deformation of the floor and the average inter-story drift; furthermore, a specific simplified methodology for the evaluation of the seismic response of URM building with flexible diaphragm is provided.

In the ASCE/SEI 41-06 document, different wood diaphragm types are defined, depending on the sheathing properties. In particular, when adopting a linear analysis procedure, suggested values for the in-plane stiffness are provided for each diaphragm category. Table 1 reports the shear stiffness (G_d) values proposed by the standard for the diaphragm types commonly used in masonry buildings, referring to both existing or retrofitted configurations. The equivalent shear stiffness of the diaphragm G_d is defined as the shear modulus multiplied by the diaphragm thickness; this definition will be adopted and used henceforth.

Single straight-sheathed diaphragms consist of single nailed sheathing laid perpendicular to the framing members; double straight-sheathed diaphragms include diaphragms

Table 1. Expected stiffness (G_d) values for some diaphragm types according to ASCE/SEI 41-06

Diaphragm type	G_d [kN/mm]
Single straight sheathing	0.35
Double straight sheathing	
Chorded	2.67
Un-chorded	1.24
Wood structural panels overlay on straight sheathing	
Un-blocked, un-chorded	0.87
Un-blocked, chorded	1.58
Blocked, un-chorded	1.24
Blocked, chorded	3.20

with a second layer of sheathing, laid either perpendicular, inclined or parallel to the first layer; existing sheathed diaphragms may be overlaid with new wood structural panels nailed or stapled to the existing sheathing and to the joists below the sheathing. The diaphragm properties are further influenced by the presence of a perimeter chord and, in the case of structural panels, with the presence of blocking in correspondence to the panel edges. The in-plane deflection at mid-span of the diaphragm (Δ) has to be evaluated in accordance to Equation 1, where ν is the shear stress multiplied by the thickness, and L is the diaphragm span, or the distance between the shear walls. Therefore, the ASCE proposal consists of defining an equivalent reference stiffness parameter (G_d) representative of the diaphragm type:

$$\Delta = \frac{\nu \cdot (L/2)}{G_d} \tag{1}$$

THE NZSEE APPROACH

The New Zealand Society for Earthquake Engineering (NZSEE) composed a guidelines document for the “Assessment and Improvement of the Structural Performance of Buildings in Earthquakes” (NZSEE 2006). This document highlights that existing masonry buildings are usually characterized by flexible diaphragms, and that it is necessary to adequately take into account this characteristic when modeling the global seismic behavior of buildings.

The document defines that “the behaviour of horizontal wood diaphragms is influenced by the type of sheathing, size and amount of fasteners, existence of perimeter chord or flange members, the ratio between the span length and the width of the diaphragm.” While the definition of the diaphragm types according to the NZSEE guidelines and to the ASCE document is almost the same, the methodology for the definition of stiffness and strength parameters follows a different approach. Indeed, the New Zealand guidelines provide formulas for the evaluation of the diaphragm stiffness depending on the properties of each component for each floor type.

In the case of square (straight) sheathing the total shear in-plane deflection at the mid-span of the diaphragm is just related to the nails slip (e_n) and can be evaluated through Equation 2, where s is the nail spacing, and L is the diaphragm span (again, the distance between the shear walls).

$$\Delta = \frac{Le_n}{2s} \tag{2}$$

In the case of panel sheathing, the NZSEE guidelines suggest evaluating the deflection at mid-span of the diaphragm by using Equation 3, where W is the lateral load applied to the diaphragm, and B is the breadth of the diaphragm. The first contribution is related to the sheathing shear deformation and obtained by assuming the sheathing as a whole element characterize by the sheathing thickness (t_P) and the shear modulus of the sheathing (G), in the hypotheses of simply supported beam and uniformly distributed load. The second contribution is related to the nail slip and is evaluated as a derivation of the board sheathing formulas, by assuming each panel as rigid; where a is the aspect-ratio of each panel and is equal to 0 if relative movement along sheet edges is prevented, and m is the number of sheathing panels along the length of the edge chord.

$$\Delta = \frac{WL}{8 \cdot GBt_P} + \frac{(1+a) \cdot me_n}{2} \tag{3}$$

From the suggestions provided by the New Zealand guidelines, it is possible to evaluate simple expressions for the equivalent shear stiffness of the diaphragm (G_d), as in Equation 4, with the same assumptions adopted by the guidelines or, rather, by approximating the diaphragm deformation as that of a simply supported beam with uniform load distribution.

$$G_d = \frac{WL}{8B} \cdot \frac{1}{\Delta} \tag{4}$$

By specifying the expressions of Δ (Equations 2 and 3) and W (as suggested by the guidelines in Appendix 11B), it is possible to obtain the next formulas for square sheathing (Equation 5) and for panels sheathing (Equation 6), where l is the joists spacing, b is the boards width, and k_n is the nails stiffness:

$$G_d = \frac{s^2 \cdot k_n}{2 \cdot l \cdot b} \tag{5}$$

$$G_d = \left(\frac{1}{Gt_P} + \frac{4sm \cdot (1+a)}{L \cdot k_n} \right)^{-1} \tag{6}$$

THE ITALIAN APPROACH

The Italian Technical Code for Construction (NTC 2008), which became effective following the 2009 Abruzzo earthquake, specifies that for existing masonry buildings, it is necessary to properly take into account both the global and local damage mechanisms. Global seismic analysis of the building has to consider, as much as possible, the real structural system. Particular attention is paid to the strength and stiffness of floors. However, with reference to wood diaphragms, the Italian Code does not specify nor does it suggest how to calculate their in-plane mechanical parameters, and the National Research Council Document on the "Instruction for design, execution and control for timber structures" (CNR DT 2006/2007) provides only a few indications regarding the mathematical hypotheses to assume, without giving any further details or instructions.

EXPERIMENTAL PROGRAM

The test apparatus was designed to reproduce, as much as possible, the actual loading and boundary conditions of an in-situ floor. In Figure 1, a schematic of the test setup is shown; the specimen loading was applied to two joists in parallel in the direction of the joists. The joists were simply supported on two external steel beams, and lateral restraints were applied on the end of each joist, restricting in-plane rotation and simulating the actual boundary conditions arising from masonry interlocking.

Because the overall stiffness of the floor unit is a combination of the in-plane stiffness of the sole diaphragm and the stiffness of the floor-to-wall shear connectors, it is considered crucial to carry out tests reproducing different actual, "real world" configurations of lateral supports. In order to distinguish these different stiffness contributions, in the first case (CC1) rigid supports were provided on the lateral joists, stopping end displacement in the load direction (Figure 1a). For the second specimen (CC2; Figure 1b), the same lateral support configuration was applied. However, a steel chord was added around the perimeter of the floor and screwed to the specimen. In the third test configuration (CC3; Figure 1c), the rigid supports on the lateral beams were removed and replaced with shear connectors providing flexible lateral support.

The configuration CC3 was designed in order to reproduce a common retrofit solution (Doglioni 2000) aimed at improving the wall-to-floor connection, consisting of providing steel elements characterized by a proper shape (i.e., L shape) on the perimeter of the diaphragm and joining these elements by means of screws or dowels to the wood joists (Figure 2). The connection with the walls is guaranteed through steel rods embedded inside the masonry that can be anchored on the external side of the wall or inside the wall thickness. This solution, simple in application, reversible and non-invasive, presents additional

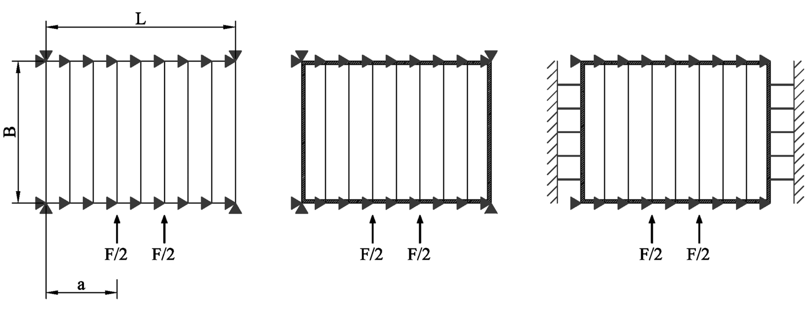

Figure 1. Test schema and different boundary conditions: (a) CC1; (b) CC2; (c) CC3.

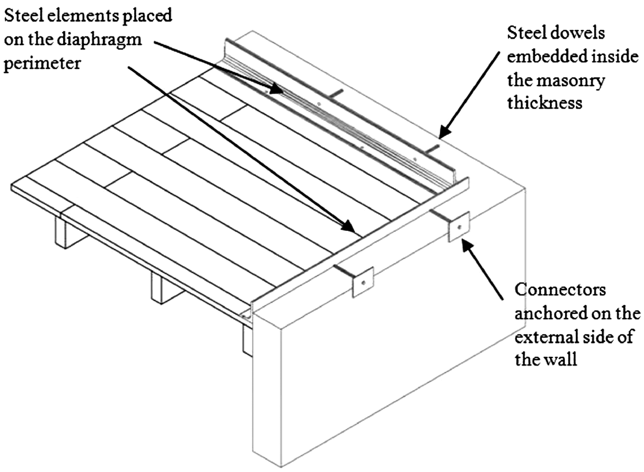

Figure 2. Wall-to-diaphragm connection through the use of L-shaped steel elements placed on the diaphragm perimeter.

advantages relating to the fact that the steel elements placed on the diaphragm perimeters lead to chord behavior, assisting the transmission of seismic actions in the diaphragm, and permit the distribution of the connection elements along the diaphragm perimeter. The condition CC2 is not actually representative of a real-world condition, and it was taken into account in order to be able to clearly identify, in the test result elaboration, the different contributions related to the addition of the steel chord and to the introduction of flexible connections.

SPECIMENS

Ten floors were tested during the experimental program, including five floors representing an as-built configuration and five floors being retrofitted through the addition of a plywood layer on the top of the floor boards. All the specimens were composed of nine rough-sawn Radiata Pine joists (50 × 250 mm) with material characteristics corresponding to No. 1 Frame Grade (visually graded) in accordance with the New Zealand Timber Structures Standard (NZS 3603-1993). The free span of each joist was 3 m, and they were spaced at 0.5 m center to center, combining to an overall width of 4 m. Square-edge straight pine flooring boards (25 × 150 mm, pine) were nailed to the joists with two standard nails (3.15 mm diameter) at each joist intersection. The flooring board layout is shown in Figure 3a. Timber flooring boards were staggered meaning that the floor was composed of a combination of 2 m and 1 m long boards. For five specimens, plywood panel overlays were screwed to the original structure. Long span structural plywood panels (2.4 × 1.2 m, 19 mm thick, 7 layers orthogonally oriented) were placed on the floor as shown in Figure 3b and fastened with gauge 8 (minimum screw shank diameter equal to 4.17 mm) × 50 mm screws spaced at 150 mm centers (average value) to

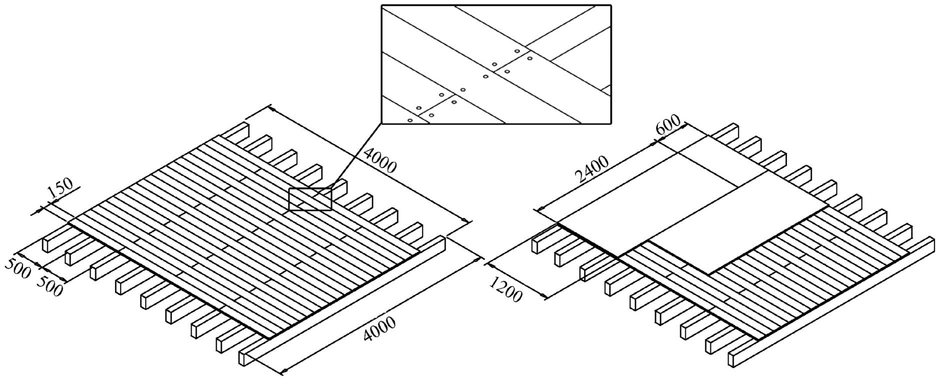

Figure 3. (a) Specimen AB-1 and (b) specimen R-1.

Table 2. Specimen characteristics

Diaphragm type	Boundary conditions CC1	CC2	CC3	CC5
Flooring boards (as-built configuration)	AB-1; AB-4	AB-2	AB-3	AB-5
Flooring boards and plywood panels (retrofitted configuration)	R-1; R-4	R-2	R-3	R-5

the flooring boards around the perimeter of each panel and with gauge 8 × 120 mm screws spaced at 150 mm centers to the joists.

In Table 2 the properties of each specimen are summarized. In the specimen configuration CC2 and CC3, steel elements were added around the diaphragm perimeter. The steel elements running parallel to the joists comprised of two steel un-equal angles (75 × 120 × 8 mm) and were attached to the decking and joists with gauge 14 (minimum screw shank diameter equal to 6.33 mm) × 100 mm long screws spaced at 150 mm centers. The steel elements running perpendicular to the joists comprised of two steel flats (75 × 8 mm) and were attached to the flooring and joists with two gauge 14 × 100 mm long screws for each joist.

The CC3 specimen configuration was characterized by flexible supports comprised of six threaded rods on each side of the floor, spaced at 500 mm, joining the two steel un-equal angles and the reaction frame. For the specimens AB-3 and R-3, two different connection configurations were applied using different mechanical properties: on the AB-3 specimen the first test was carried out, adopting 12 mm Φ, mild steel (class 4.6) threaded rods; after the test the connectors were removed and substituted with 12 mm Φ, high-strength (class 8.8) threaded rods; on the R-3 specimen 12 mm Φ, high-strength threaded rods were used during the first test, then replaced by 16 mm Φ, high-strength, threaded rods during the second test.

The retrofit solution applied on the AB-5 and R-5 specimens (CC5) consisted of the application of metal sheet-blocking (gauge 24 - thickness equal to 0.6 mm - $\times$75 mm wide) stapled (gauge 16 staples, spaced at 60 mm centers) between the flooring boards or between the plywood panels. In the AB-5 specimen metal blocking was placed directly on the boards, joining the boards in pairs.

In diaphragm R-5, the steel blocking joined the plywood panels around the edges, with the aim of making the plywood diaphragm homogeneous. (i.e., as if only a single plywood sheet was used).

TEST SETUP

A general view of the experimental setup is shown in Figure 4. A three-dimensional steel frame was designed and built in order to support both lateral and gravity loading (Figure 4a, Figure 4c). Four steel columns were fixed to the reaction floor and connected to four steel beams: two were placed orthogonally to the loading direction, with the joists being simply supported on them; the other two were placed parallel to the load direction, providing lateral support for the diaphragm specimen. The contact between the timber joists and the steel beams was composed of small sphere transfer units and steel plates, permitting the sliding of the specimen on the gravity load supports and minimizing friction forces (Figure 4d). In order to avoid the in-plane rotation of the joist, lateral supports at both ends of each joist were attached using two steel angles for each joist (Figure 4d).

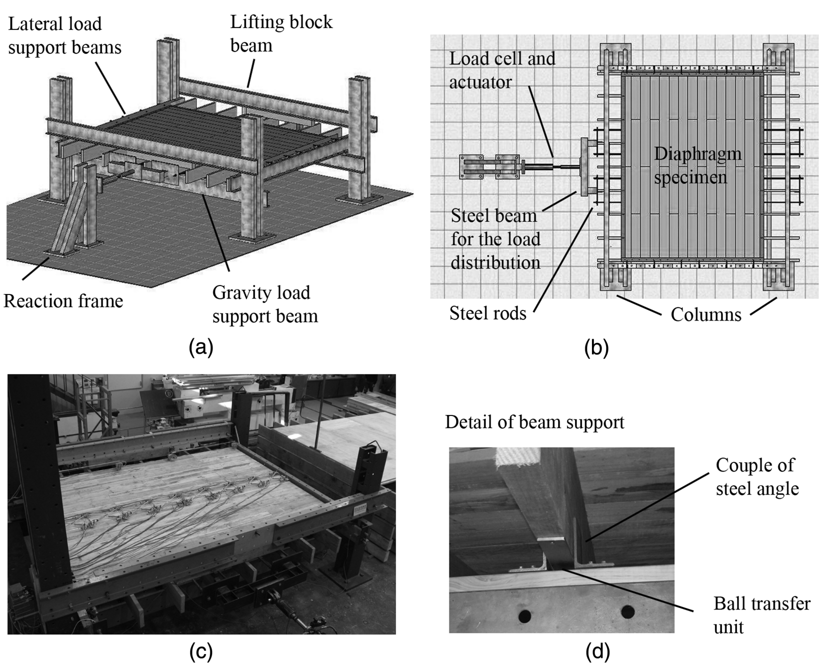

Figure 4. Test setup (drawings by Laurent Coutagne).

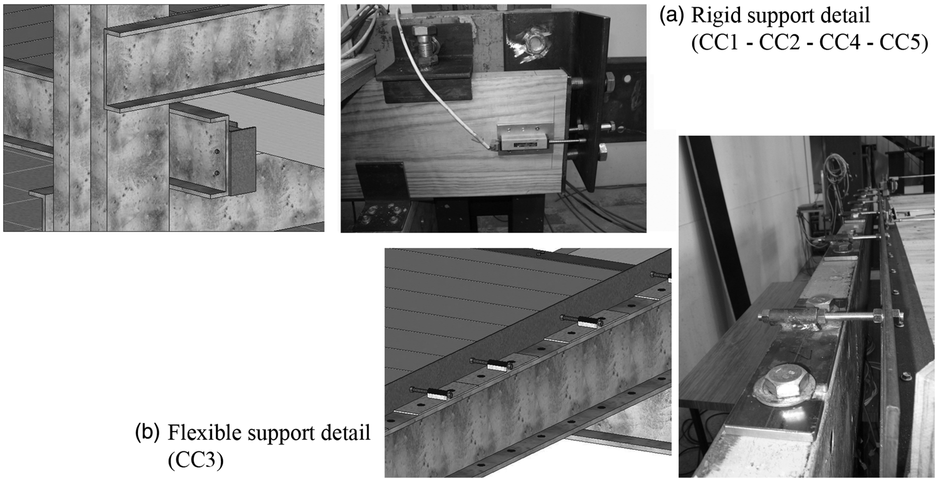

Figure 5. Details of the lateral supports at the joists' extremity.

Lateral support was achieved in different manners depending on the differing test requirements. Where rigid support was required, the lateral displacement of joists was avoided, with steel angles placed at the end of the external joists and connected to the external frame (Figure 5a). For the specimens AB-3 and R-3, flexible shear connectors were placed between the steel perimeter chord and the lateral supports; a detail of this fitting is shown in Figure 5b. The free length of the connectors was designed to be equal to 5 times the diameter of the rods, in order to reproduce the flexural and shear behavior of connectors embedded with cement grout within a scabbled stone masonry with good bonding (Piazza et al. 2006). In the Proposed Approach section below, the implication of this assumption on the test results will be discussed.

In order to apply the quasi-static cyclic load, a 200 kN-capacity hydraulic actuator was attached to a steel loading frame connected to two joists and to a reaction frame, which was bolted to the strong floor. Two steel plates were placed at the extremities of each loaded joist and connected with two steel rods to ensure transfer of the horizontal load to the opposite side of the diaphragm, thus enabling the pulling action (Figure 4b). The applied lateral displacements were measured by a rotary potentiometer while the resulting forces were measured directly through the actuator's built-in load cell.

The specimen response was obtained from linear variable displacement transducers (LVDTs) and rotary potentiometers. These instruments were used to measure the contribution of each elements response to the overall specimen response. The common arrangement of these instruments for all the tests is shown in Figure 6. Seven rotary potentiometers and two LVDTs (lateral joists) were placed at the end of the joists (one for each joist), on the side of the diaphragm opposite to the actuator, in order to measure the displacement in the load direction (relative to the lateral support) and define the global deformed shape of the floor. In order to measure the shear deformation of the floor, 4 rotary potentiometer were placed diagonally between the loaded and lateral joists. In addition a series of 42 LVDTs were placed as shown in Figure 6, to investigate the local shear deformation of the floor.

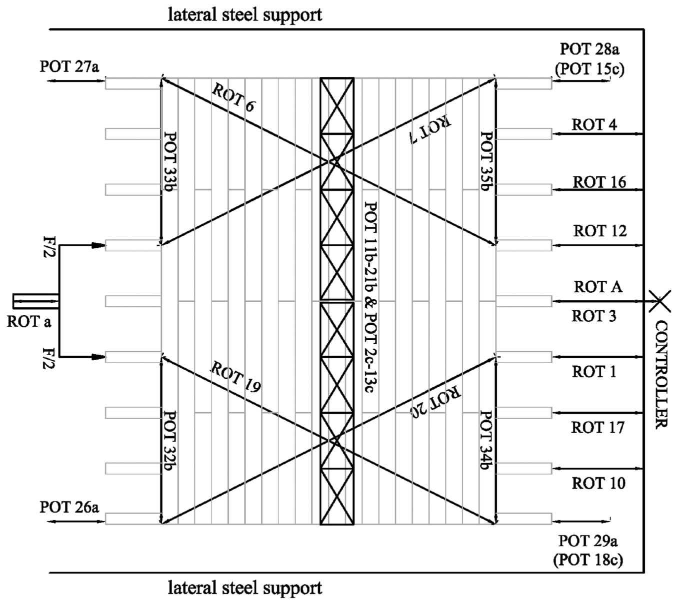

Figure 6. Instrumentation arrangement.

LOADING PROTOCOL

Displacement-controlled, quasi-static, reversed cyclic testing was performed on each diaphragm applying the displacement with the actuator in incremental displacement amplitudes. The load protocol (Figure 7) was defined starting from the suggestion given by the European Standard EN 12512-2003: One or two cycles for each lateral displacement amplitude (3 mm, 6 mm, 12 mm, 30 mm, 40 mm, 60 mm, 80 mm, and 100 mm) were applied, the displacement amplitudes were determined as percentage of the maximum predicted displacement. The loading rate ranged from 0.1 mm/s to 0.2 mm/s for the lowest and highest amplitude cycles, respectively.

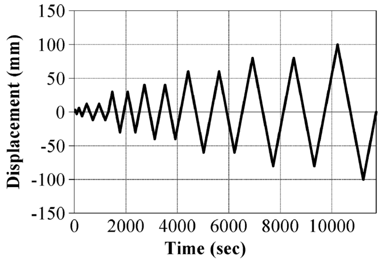

Figure 7. Displacement control load pattern.

TEST RESULTS

IN-PLANE STIFFNESS RELATED TO THE SYSTEM DIAPHRAGM PLUS LATERAL CONNECTIONS

Figure 8a shows a comparison between load versus the mid-span displacement curves of specimens AB-1 and R-1. Significant residual displacements occur due to the inelastic response when the load is reduced to zero. When the load is reversed, the loop shows a low initial shear stiffness, and it gradually increases as the load increases, until the response is similar to the initial load cycle. This phenomenon is known as pinching and is attributed to the slack in nail joints, associated with local damage to the wood in the vicinity of the connectors (Zagajeski et al. 1984).

For the specimen AB-1, up to a lateral displacement of 3 mm an initial uniform stiffness of 1.7 kN/mm was achieved during loading. On the next displacement increment, the tangent stiffness reduced to 0.7 kN/mm, remaining nearly constant until a maximum load of 55 kN. The residual displacement grew after each cycle, with a maximum of 13 mm for pull-cycles and 26 mm for push-cycles (20 mm on average). The failure mechanism, which occurred upon reaching 100 mm displacement, affected the flooring boards' flexural resistance. Figure 9a shows the diaphragm's deformed shape obtained from the rotary potentiometers

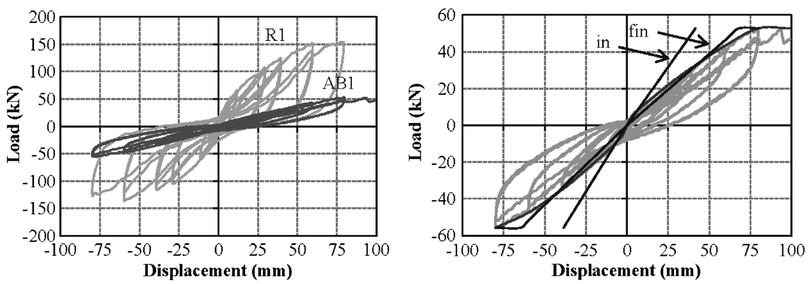

Figure 8. Load versus displacement curves. (a) As-built and retrofitted specimens AB-1 and R-1; (b) evaluation of backbone curve and initial and final deformation of the diaphragm AB-1.

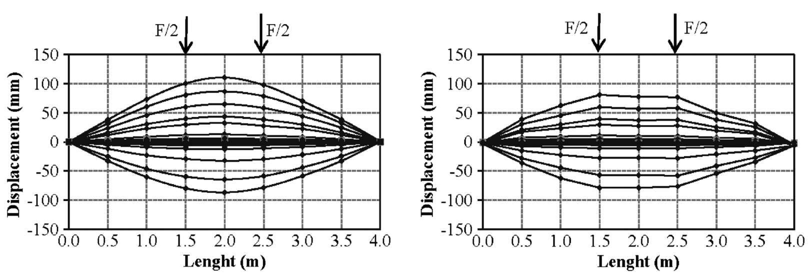

Figure 9. Deformed shape for different load cycles. (a) As-built specimens AB-1; (b) retrofitted specimens R-1.

placed on the joists. The displacement measures of each cycle are plotted in order to show the deformed shape at lateral displacement increasing. It is possible to note that the diaphragm deformation is comparable to a flexural deformed shape arising from the flexural deflection of the flooring boards.

The load-versus-displacement curve related to the specimen R-1 underlines that the effect of the plywood panel overlays results in a significant increase in both diaphragm strength and stiffness; the maximum load reached during the test is equal to 150 kN, and it is three times of that related to the as-built specimen. The curve shows a strong nonlinearity after the first load cycles, proving that the diaphragm behavior is strongly affected by the connection between the wood elements (nails and screws). The residual displacement was observed from the first cycle and remained almost constant during the successive cycles, with a maximum of 25 mm. The failure mechanism occurred at a displacement of 80 mm and principally affected the screws between panels and boards (short screws) and between panels and joists (long screws). Figure 9b shows the diaphragm deformed shape obtained from the rotary potentiometer placed on the joists. In this case, it is possible to recognize that the global deformation of the floor is mainly characterize by shear deformation.

For each test, the backbone curves have been plotted, in order to highlight the characteristic features of the in-plane shear force versus mid-span displacement response of wood diaphragms. These curves clearly show the nonlinear behavior of the diaphragm specimens (as previously highlighted) which are crucial in defining a value of shear stiffness related to a significant displacement level (associated to a limit state). In particular, it is important to evaluate an *initial* stiffness value (*in*) related to a low displacement level (12 mm) and a somehow *final* value (*fin*) related to the maximum displacement reached during the test. The *final* stiffness value is evaluated using an equivalent bilinear curve characterized by the same energy absorption of the real system (Figure 8b).

Figure 10 summarizes and compares the backbone curves related to all the specimens. For both the floor systems with straight flooring boards or the reinforced with plywood panel overlays, it is possible to observe that the addition of steel elements on the perimeter (CC2) leads to an increase both in terms of strength and stiffness with respect to the base configuration (CC1), while the influence of flexible connections (CC3) leads to a reduction especially in terms of ductility and strength, due to the occurrence of failure mechanisms in the connectors. On the other hand, the use of steel strips for reducing the relative slip between

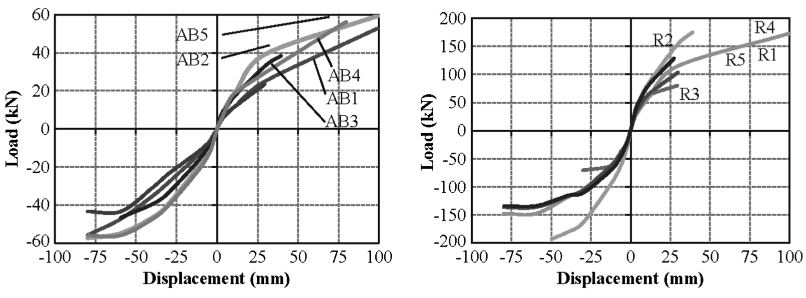

Figure 10. Comparison between backbone curves for all specimens.

Table 3. Main test results

Specimen	d_{max} [mm]	F_{max} [kN]	Failure mode
AB-1	100	55	Boards
AB-2	100	60	Boards and steel
AB-3 test1	60	45	Connectors
AB-4	80	45	Boards
AB-5	80	55	Staples and boards
R-1	80	150	Screws
R-2	55	200	Screws
R-3 test1	30	80	Connectors
R-3 test2	40	140	Connectors
R-4	100	175	Screws
R-5	80	150	Staples and screws

wood elements (boards or plywood panels; CC5), leads to an increasing of initial stiffness, while the panels strength is identical to specimens without metal blocking. The main test results are summarized in Table 3.

In order to obtain results independent from geometry and dimensions of the specimen, it is necessary to evaluate equivalent stiffness parameters. Starting from the load versus mid-span displacement curve, it is possible to evaluate the equivalent shear stiffness (G_1) in accordance with the theory proposed by Timoshenko (1921), without taking into account for the flexural component of the deformation as shown in Equation 7, where a is the distance between the load application and the lateral supports and F is the applied load (Figure 1).

$$G_1 = \frac{F/2}{B} \cdot \frac{a}{\Delta} \tag{7}$$

It is worth nothing that with this assumption, the defined parameter G_1 is comparable to the parameter G_d introduced in the previous chapter, despite the different load configuration adopted in the test setup.

LATERAL CONNECTORS STIFFNESS

Figure 11 shows a comparison between the connectors behavior, displaying the load versus displacement curves relative to the mean displacement of the lateral beams. With reference to the first test carried out on the as-built specimen AB-3, up to a displacement of 1 mm, the connections displayed an elastic behavior. At the next displacement increment, the curve stiffness changed as the connectors entered the post-yield region, until a maximum load of 45 kN. Fracture occurred during the next load cycle at a lower load equal to 27 kN. After the previous test, the broken connectors were removed and replaced with stronger connections (high-strength steel, class 8.8), and a second test was carried out on the same specimen. The comparison between the connector behavior during test 1 and test 2 highlights that during the second test, the high strength connectors remained in the elastic range and showed the same stiffness as the connectors used for the previous test.

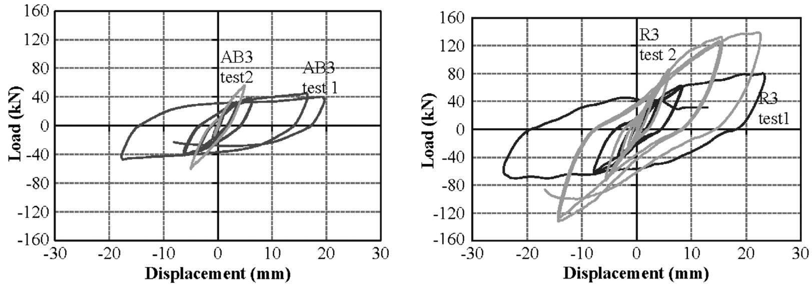

Figure 11. Load versus lateral beams displacement curves, for AB3 and R3 tests with lateral flexible connectors.

For the retrofitted specimen R-3 the maximum displacement measured on the lateral joists is approximately that which was measured at the central joist (Figure 12), showing that most of the system deformation is concentrated at the lateral connection. During the first load cycle, the connection behaved elastically. During the following displacement increment, the curve surpassed the yield point and the connectors reached a maximum load of 80 kN. System failure occurred during the second load cycle at a lower load equal to 45 kN. A second test was carried out on specimen R-3 after the substitution of the broken connectors with stronger elements (14 mm Φ threaded rods, high strength steel, class 8.8). The comparison between the connectors' behavior during test 1 and test 2 shows that during the second test, the stronger connectors could sustain higher load values (140 kN, 22 mm) and the failure occurred in the following cycle at a lower load of 100 kN (11 mm).

From the displacement transducers located on the external joists, it is possible to evaluate the lateral connectors stiffness (k_c), adopting Equation 8, where d_M is the mean value of the data measured during each load step by the displacement transducers located on the lateral beams.

$$k_C = \frac{F/2}{d_M} \tag{8}$$

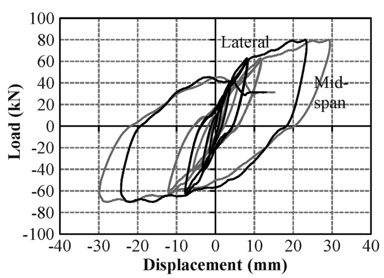

Figure 12. Lateral and mid-span displacement versus load for specimen R3_test1.

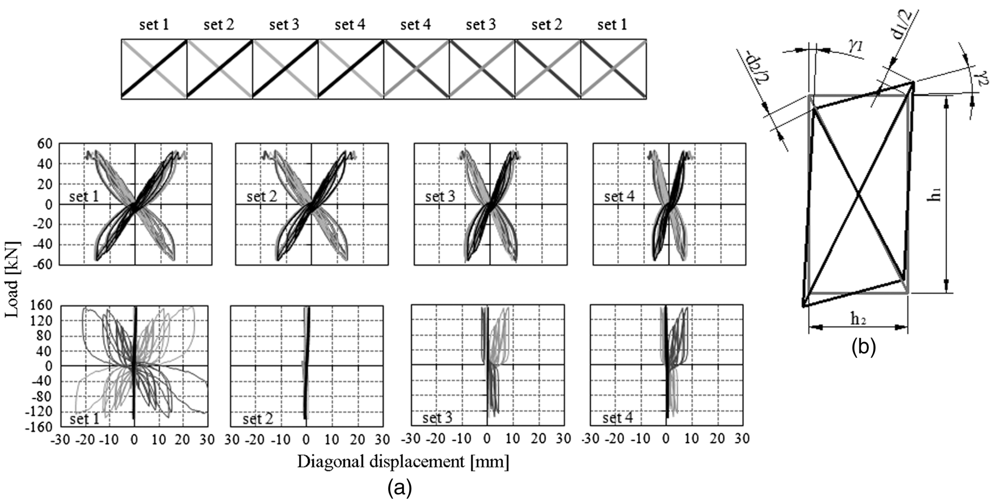

Figure 13. Angular deformation of instrumented regions: (a) Diagonal displacement versus load for diaphragm AB-1 and R-1; (b) evaluation of angular deformation.

STIFFNESS OF THE DIAPHRAGM TOP LAYER

Starting from the displacement measured from the rotary potentiometers located on the floor diagonals and from the crossed LVDTs placed in the mid-section of the diaphragm (Figure 6), it is possible to evaluate the angular deformation of the diaphragm top layer. Figure 13a shows the displacement measured from the crossed LVDTs versus the applied load, for both specimens AB-1 and R-1. For the as-built specimen AB-1, the diagonal displacements related to the external part of the diaphragm (Set1, Set2) are bigger and decrease toward the center of the diaphragm (Set3, Set4), coherently to the in-plane bended beam type deformation. On the contrary, for the retrofitted specimen R-1, the top layer deformation is concentrated in the panel joints and the potentiometers bridging the panel joints measured consistent diagonal displacement, while those located on the same panels registered close to zero displacement throughout the test.

Starting from these measurements, it is possible to evaluate the local shear deformation (γ) for each rectangular instrumented region (Figure 13b) by using the Equation 9, where h_1 and h_2 are the dimensions of the instrumented region, d_1 and d_2 are the relative extension or shortening of the two diagonals (d_1 is positive and d_2 is negative when F is positive, and vice versa), while the redundant measures of extension and shortening of the perimeter gauges were used for a cross-checking of the results. In the same way, it is possible to evaluate the shear deformation starting from the diagonal displacement measured from the rotary potentiometers. This data provides a global angular deformation value, related to each diaphragm portion between lateral and loaded beams.

$$\gamma = \gamma_1 + \gamma_2 = \frac{\sqrt{h_1^2 + h_2^2}}{h_1 \cdot h_2} \cdot \frac{d_1 - d_2}{2} \tag{9}$$

Table 4. Stiffness parameters related to initial (*in*) and final (*fin*) displacement.

Specimen	G_1 [kN/mm]		G_2 [kN/mm]		G_3 [kN/mm]	
AB-1	0.34	0.20	0.36	0.22	0.36	0.22
AB-2	0.49	0.30	0.58	0.32	0.53	0.32
AB-3 test1	0.44	0.28	0.49	0.34	0.48	0.33
AB-4	0.33	0.20	0.33	0.20	0.32	0.20
AB-5	0.52	0.32	0.60	0.37	0.65	0.41
R-1	1.66	0.90	5.57	2.21	5.62	2.51
R-2	2.36	1.46	6.91	3.37	6.11	3.55
R-3 test1	1.69	1.31	7.20	6.51	6.15	5.41
R-3 test2	1.93	1.46	5.54	4.59	4.96	3.50
R-4	1.60	0.87	np	np	2.91	2.29
R-5	1.99	1.12	14.1	3.69	10.1	3.67
	in	*fin*	*in*	*fin*	*in*	*fin*

For evaluating the equivalent shear stiffness (G_2 and G_3) of the top layer of the floor, both starting from global and local deformation data, it is possible to use Equation 10, where $\gamma_{M,glob}$ and $\gamma_{M,loc}$ are the average values of the angular deformations measured by diagonal rotary potentiometers and LVDTs, respectively (Figure 6).

In Table 4, the experimental results for each test are summarized. Secant equivalent shear stiffness parameters relative to both the initial (*in*) and final (*fin*) condition are reported in order to characterize the nonlinear behavior of each diaphragm (Figure 8b). The measured values of G_2 and G_3 are similar: a difference of around 10% is noted for both joist and board configurations (AB-i) and for the floors with the plywood layer on the top (R-i), highlighting that the global measurements are congruent with the mean values of the local ones.

$$G_2 = \frac{F/2}{B \cdot \gamma_{M,glob}} \quad ; \quad G_3 = \frac{F/2}{B \cdot \gamma_{M,loc}} \tag{10}$$

The comparison between the parameter G_1 and the parameters G_2 and G_3, shows that while for the as-built specimens the difference between the equivalent stiffness relative to the whole system (G_1) and that relative to the top layer of the floor (G_2 and G_3) is not significant (around 10%), in the case of the specimens with the plywood panel overlays, the difference increases significantly. In these six cases, the ratio between G_2 or G_3 and the equivalent stiffness G_1 is around 300%, showing that the addition of plywood panels leads to a concentration of deformation in the elements (nails and screws) connecting the top layer of the floor and the joists.

MATHEMATICAL MODELING FOR THE EVALUATION OF DIAPHRAGM STIFFNESS

COMPARISON BETWEEN EXPERIMENTAL RESULTS AND THEIR PREDICTIONS

The values obtained from the experimental results presented in the previous section can be compared to those obtained using the current standards/guidelines previsions. Figure 14

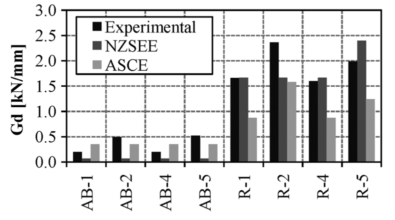

Figure 14. Shear stiffness values. Comparison between experimental and code-predicted results.

represents a graphical comparison between the experimental results carried out during the experimental research previously described and those predicted using the NZSEE or the ASCE documents.

Referring to the straight flooring boards' diaphragm type, both the ASCE and NZSEE approaches suggest methodologies for the prediction of the shear stiffness. For this floor type, the experimental results are better represented by the values proposed by the ASCE document, while the NZSEE guidelines seem to underestimate the effective shear stiffness values, underlining that rigid rotation of each board segment, due to nail slip, is not the sole contribution to the shear stiffness and it is too conservative to neglect the contribution related to boards interlocking and friction at the boards edges.

The comparison between the experimental results related to the floor type characterized by plywood panel overlays on the existing flooring boards (R-i) and the predicted results highlights that the shear stiffness in the case of this retrofit solution depends on a large number of parameters, and it is thus difficult to properly characterize the floor behavior by assigning a reference value related to a particular category. For this reason, the ASCE suggestions appear not to be well representative, while the NZSEE guidelines seems better able to represent the results. It is worth noting that Equation 3, adopted for the prediction of stiffness values, is actually referred to a panel sheathing directly connected to the joists without the presence of flooring boards, but can be representative of the floor type analyzed because of the low contribution of the existing flooring boards to the total shear stiffness.

It is worth noting that neither the NZSEE and the ASCE provisions are able to predict the stiffness contribution related to the shear wall-to-floor connectors, even if Table 4 highlights that it is quite important to take into account this contribution.

PROPOSED APPROACH

The analyses of experimental results and the comparison with predictions achievable by using different codes are used as basis for defining a consistent methodology for the evaluation of diaphragms stiffness. Figure 15 shows that the overall stiffness of the floor unit $(k_{eq,c+d})$ is given by the contribution of the in-plane stiffness of the sole diaphragm $(k_{eq,d})$ and the stiffness of floor-to-wall shear connectors (k_c), where F is the total seismic action (Brignola et al. 2009a). The two systems (diaphragm and connectors) are in series, and the total displacement at mid-span of the diaphragm (Δ) is given by the sum of the

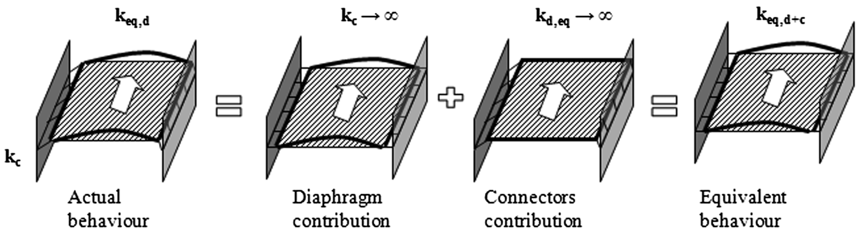

Figure 15. Schematic contributions of connectors and diaphragm stiffness to the overall floor system stiffness.

two contributions due to the stiffness of the shear connectors (Δ_c) and the diaphragm stiffness (Δ_d).

The shear stiffness G_{d+c} related to the whole system (i.e., diaphragm and connectors) can be defined from the effective stiffness by using Equation 11. It is thus important to correctly define both the contributions of the diaphragm-only shear stiffness (G_d) and of the connector stiffness (k_c), before and after the strengthening intervention to obtain a proper assessment and retrofit design of a masonry building.

$$G_{c+d} = \frac{L}{4B} \cdot k_{eq,c+d} = \frac{L}{4B} \cdot \left(\frac{1}{k_{eq,d}} + \frac{1}{k_{eq,c}}\right)^{-1} = \left(\frac{1}{G_d} + \frac{4B}{Lk_c}\right)^{-1} \tag{11}$$

For stud connectors embedded inside the masonry, the stiffness contribution can be evaluated as suggested by Piazza and Baldessari (2006) on the basis of the experimental results from the University of Brescia (Giuriani et al. 1993, Felicetti et al. 1997). This assumes dowel behavior for each connector and summarizes the masonry type and anchorage techniques into a parameter n calibrated from the experimental results. For connectors embedded with cement grout within stone masonry the parameter n can range, according to the referenced experimental results, between 3 to 7, depending on the masonry quality (low values for dressed rectangular stone masonry and higher values for irregular stone masonry). If N is the number of connectors for each wall, E is the connector's Young modulus, and D is the diameter, the stiffness is given by:

$$k_c = N \cdot \frac{3}{16} \cdot \frac{\pi E D}{n^3} \tag{12}$$

The diaphragm-only stiffness (G_d) depends on the diaphragm type and details. For straight flooring boards only (as-built), both the ASCE and NZSEE documents seem to reproduce inadequately the experimental results. From the experimental observation of the diaphragm behavior (Figure 16), it is thus assumed that each board contributes to the load carrying as a simply supported beam characterized by the transversal section $b \times t_{B,}$ if boards span the full diaphragm length (L) or if sufficient interlocking is guaranteed between boards. The continuity of boards at the joists intersection determine that the nails effect cannot be assumed as the NZSEE document suggest: the moment of forces generated by nail couples at

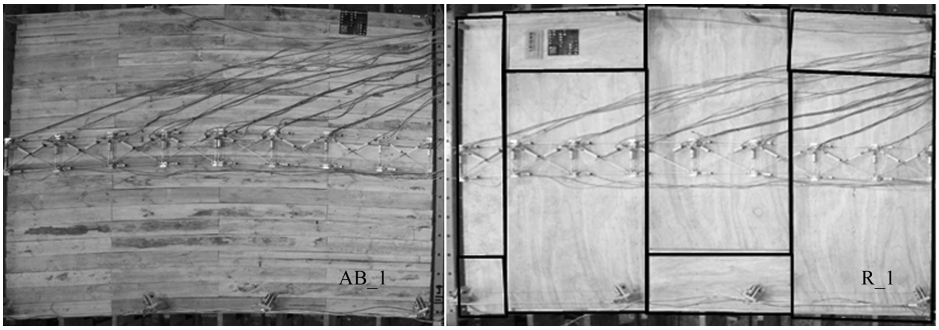

Figure 16. Experimental deformed shape for the specimen AB-1 and R-1.

each joists is not able to limit significantly the boards rotation and the effect of the concentrated rotational springs is then neglected. The chord action gives rise to a double effect on the diaphragm system stiffness: first, the two steel elements placed orthogonally to the seismic load work in parallel with the boards and the total stiffness, for the evaluation of the bending deflection in the mid-span of the diaphragm, comprises of a portion related to these elements stiffness; second, the two steel elements, parallel to the shear resisting walls and welded with the other chord elements, provide a semi-rigid rotational joint to the diaphragm.

The mathematical model assumed for describing the AB-2 specimen (as-built with chord) is represented in Figure 17. Parallel simply supported elements characterized by flexural behavior (the shear deformation is neglected) represent the central boards, while the lateral boards and the steel elements, to which they are connected, are simplified as beams with two fixed joints at the extremity. All these elements are assumed to work in parallel and contribute to carry different portions of the total load W: W_c is the amount carried by each chord element

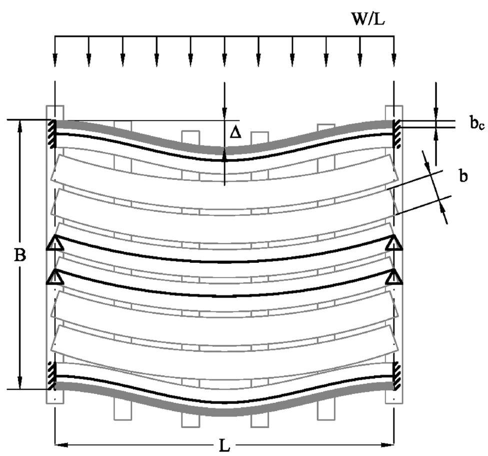

Figure 17. The mathematical model assumed for representing the AB-2 specimen.

orthogonal to the seismic action, W_{b1} is the amount carried by each external board, and W_{b2} is the amount carried by each internal board. With these assumptions, it is possible to obtain Equation 13 for the full characterization of the diaphragm stiffness, where E_B is the elastic modulus of the wooden boards; b_C and t_c are the section dimensions of the perimeter steel chord; E_c is the steel Young modulus; L and B are the diaphragm dimensions.

$$G_d = \frac{WL}{8B} \cdot \frac{1}{\Delta} = \frac{4b^2 E_B t_B}{5L^2} + \frac{32b^3 E_B t_B}{5L^2 B} + \frac{8b_C^3 E_C t_C}{L^2 B} \tag{13}$$

In relation to the diaphragm type composed of straight flooring boards and plywood panel overlays (retrofitted), in the absence of the perimeter chord, the specimens tested (R-1 and R-4) are very well represented by the NZSEE (Figure 14). Also, in this case, the chord contribution has two different effects: first of all the chords presence prevents the relative movement between the sheet edges and the New Zealand guidelines suggest to assume the parameter a related to the panel ratio, equal to zero; the second contribution is related to the beam action of the chord elements orthogonal to the seismic action. The contribution to the total stiffness can be evaluated in analogy to the straight flooring board diaphragm type, by considering the diaphragm and the two chord elements in parallel. Again the chord is evaluated as a fixed-fixed–ended beam and congruence of deflection at the mid-span of the diaphragm is imposed. The total shear stiffness can thus be evaluated with Equation 14, where G is the panel shear modulus and t_P is the panel thickness; a is the aspect-ratio of each panel and is equal to 0 if relative movement along sheet edges is prevented, m is the number of sheathing panels along the length of the edge chord, s is the nails spacing and k_n is the nail stiffness.

$$G_d = \left(\frac{1}{Gt_P} + \frac{4sm(1+a)}{Lk_n} \right)^{1} + \frac{8b_C^3 E_C t_C}{L^2 B} \tag{14}$$

Figure 18a represents the comparison between the experimental results and the values obtained by using the Equations 13 and 14 previously presented. It is comforting to note that the assumed mathematical modeling effectively well represent the shear stiffness actually measured during the experimental campaign. Furthermore, Figure 19 represents the different contribution related to chords, panels and boards, combining the total diaphragm shear stiffness, both for experimental results and analytical formulas. It is important to note that the

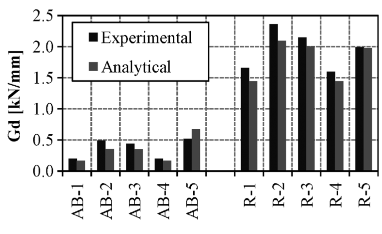

Figure 18. Comparison between experimental results and their prediction through the proposed analytical formula.

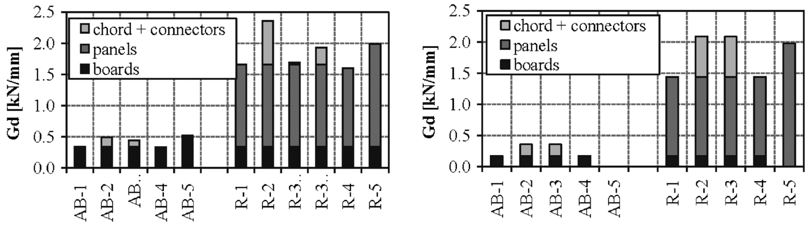

Figure 19. Comparison between (a) experimental results and (b) their predictions, focusing on the contribution of different elements.

connector's contribution is herein not independently summed to the other components, but it is plotted in the histograms together with the chord contribution. However, the final results for specimens AB-3 and R-3 take into account the connectors contribution.

CONCLUSIONS

The results of an experimental program carried out at the University of Canterbury as a joint project with the University of Genoa, comprising an experimental investigation on different diaphragm configurations subjected to quasi-static cyclic loading, were presented and discussed. The experimental program was designed with the aim of achieving results where it was possible to distinguish the different contributions of each component of the floor system. Particular attention was given to the evaluation of the diaphragm-only stiffness and the stiffness of the connectors by carrying out tests on specimens characterized by different boundary conditions. Stiffness values related to the initial phase of testing and a secant value representative of the collapse state were obtained, clearly highlighting the nonlinear behavior of floors. Furthermore, due to the large amount of instrumentation placed on the specimens during testing, it was possible to obtain an indication of the stiffness contributions due to nails and screws and the wood elements deformability (boards and panels).

In terms of timber diaphragm in-plane stiffness, the experimental results have been compared to those predicted by using different international guidelines and standards, highlighting both the shortcomings and qualities of each approach analyzed. Following the deformation mechanisms observed during the tests, some modifications to the mathematical models currently proposed by codes and guidelines, and a simplified formulation for the evaluation of the stiffness properties of timber diaphragm have been proposed. In particular, a mathematical model based on a beam analogy for each board was used for the straight flooring boards diaphragm, finding results better fitted to the experimental one, compared to both the American and New Zealand previsions. Also, for the diaphragm type with plywood panels overlaid on the flooring boards, the New Zealand proposal was well representative, and modifications related to steel chord and lateral connectors were added to the mathematical model proposed in the NZSEE document.

This paper principally focused on the role of the initial in-plane stiffness of few diaphragm types in the direction parallel to the joists. Further research is necessary, aimed at investigating the other direction's response and at the other mechanical properties that describe the in-plane behavior of the wood floors, affecting the global seismic behavior of masonry buildings, such as the stiffness degradation, the shear strength and the energy dissipation.

ACKNOWLEDGMENT

The authors acknowledge the New Zealand Foundation of Research, Science and Technology (FRST) for the research funds provided to support the experimental component of this research, as part of the Project “Retrofit Solutions for NZ Multi-storey Buildings”.

REFERENCES

American Society of Civil Engineers (ASCE/SEI 31-03), 2003. *ASCE/SEI 31-03: Seismic Evaluation of Existing Buildings*, Reston, VA.

American Society of Civil Engineers (ASCE/SEI 41-06), 2007. *ASCE/SEI 41-06: Seismic Rehabilitation of Existing Buildings*, Reston, VA.

Brignola, A., 2009. Evaluation of the In-Plane Stiffness of Timber Floors for the Performance-Based Retrofit of URM Buildings, Ph.D. Thesis, University of Genoa, Italy.

Brignola, A., Pampanin, S., and Podestà, S., 2009a. Evaluation and control of the in-plane stiffness of timber floors for the performance-based retrofit of URM buildings. *Bulletin of the New Zealand Society for Earthquake Engineering* **42**, 204–221.

Brignola, A., Pampanin, S., and Podestà, S., 2009b. The role of the in-plane stiffness of timber floors in the seismic response of unreinforced masonry buildings, *Proc. of the Prohitech Conference 2009*, 21-24 June 2009, Rome, Italy. Volume **II**, 1253–1261.

Brignola, A., Pampanin, S., and Podestà, S., 2010. A retrofit strategy for unreinforced masonry buildings accounting for the in-plane stiffness of timber diaphragms, *Proc. of 14th European Conference of Earthquake Engineering*, Ohrid (Macedonia), September 2010, CD-ROM.

Consiglio Nazionale delle Ricerche (CNR-DT 206), 2007, *Istruzioni per la progettazione, l’Esecuzione e il Controllo delle Strutture in Legno*, Rome (in Italian).

Corradi, M., Speranzini, E., Borri, A., and Vignoli, A., 2006. In-plane shear reinforcement of wood beam floors with FRP, *Composites* Part B, **37**, 310–319.

Decreto Ministeriale delle infrastrutture (D.M. 14-01-2008), 2008. *Norme Tecniche per le Costruzioni*. NTC 2008 (in Italian).

Latvian Standards (EN 12512-2003), 2003. Timber structures - Test methods - Cyclic testing of joints made with mechanical fasteners, Standardisation Bureau Latvian Standards, Riga, Latvia.

Doglioni, F., 2000. Handbook (guidelines) for the design of adjustment interventions, seismic strengthening, and renewal of architectural treasures damaged during the Umbria-Marche earthquake in 1997, Official Bulletin of Marche Region, Ancona (in Italian).

Felicetti, R., Gattesco, N., and Giuriani, E., 1997. Local phenomena around a steel dowel embedded in a stone masonry wall, *Materials and Structures* **30**, 238–246.

Gattesco, N., Macorini, L., and Benussi, F., 2007. Retrofit of wooden floors for the seismic adjustment of historical buildings with high reversible techniques, Seismic Engineering in Italy, *Proc. of the XII National Conference*, Pisa, 10–14 June 2007, full paper on CD (in Italian).

Giuriani, E., Gattesco, N., and Del Piccolo, M., 1993. Experimental tests on the shear behavior of dowels connecting concrete slabs to stone masonry walls, *Materials and Structures* **26**, 293–301.

New Zealand Society for Earthquake Engineering (NZSEE), 2006. *Assessment and Improvement of the Structural Performance of Buildings in Earthquake*, Recommendations of a NZSEE Study Group, Wellington, New Zealand.

Paquette, J., and Bruneau, M., 2006. Pseudo-dynamic testing of unreinforced masonry building with flexible diaphragm and comparison with existing procedures, *Constructions and Building Materials* **20**, 220–228.

Peralta, D. F., Bracci, J. M., and Hueste, M. B. D., 2004. Seismic behavior of wood diaphragms in pre-1950s unreinforced masonry buildings, *Journal of Structural Engineering* **130**, 2040–2050.

Piazza, M., and Baldessari, C., 2006. *Interazione di solai lignei con elementi portanti in muratura di edifici esistenti*, ReLUIS-DPC 2005-2008 Report intermedio del progetto di ricerca (in Italian).

Piazza, M., Baldessari, C., and Tomasi, R., 2008. The role of in-plane floor stiffness in the seismic behavior of traditional buildings, *Proc. of 14th World Conference on Earthquake Engineering*, Beijin 12–17 October 2008, CD-ROM.

Tena-Colunga, A., 1992. Seismic evaluation of unreinforced masonry structures with flexible diaphragms, *Earthquake Spectra*, **8**(2): 305–318.

Tena-Colunga, A., and Abrams, D.P., 1996. Seismic behavior of structures with flexible diaphragms, *ASCE Journal of Structural Engineering* **122**, 439–445.

Timoshenko, S. P., 1921. On the correction factor for shear of the differential equation for transverse vibrations of bars of uniform cross-section, *Philosophical Magazine*, p. 744.

Zagajeski, S., Halvorsen, G. T., Ganga Rao, H. V. S., Luttrell, L. D., Jewell, R. B., Corda, D. N., and Roberts, J. D., 1984. *Theoretical and Experimental Studies on Timber Diaphragms Subject to Earthquake Loads*, Final Summary Report, Department of Civil Engineering, West Virginia University, Morgantown, WV.

(Received 18 September 2010; accepted 13 January 2012)

Queries

1. This query was generated by an automatic reference checking system. This reference could not be located in the databases used by the system. While the reference may be correct, we ask that you check it so we can provide as many links to the referenced articles as possible.
2. This query was generated by an automatic reference checking system. This reference could not be located in the databases used by the system. While the reference may be correct, we ask that you check it so we can provide as many links to the referenced articles as possible.